Geoderma Regional 40 (2025) e00905

Contents lists available at ScienceDirect

Geoderma Regional

journal homepage: www.elsevier.com/locate/geodrs

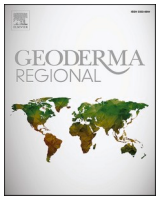

Mapping soil parent materials in a previously glaciated landscape: Potential for a machine learning approach for detailed nationwide mapping

Yiqi Lin [a,*], William Lidberg [a], Cecilia Karlsson [b], Gustav Sohlenius [b], Florian Westphal [a,c], Johannes Larson [a], Anneli M. Ågren [a]

[a] Department of Forest Ecology and Management, Swedish University of Agricultural Sciences, Skogsmarksgränd 17, 901 83 Umeå, Sweden
[b] Geological Survey of Sweden, Villavägen 18, 752 36 Uppsala, Sweden
[c] Department of Computing, Jönköping University, Gjuterigatan 5, 553 18 Jönköping, Sweden

ARTICLE INFO

Keywords:
Digital soil mapping
Soil parent materials
Airborne laser scanning
Machine learning
Extreme gradient boosting

ABSTRACT

Reliable information on soil-forming parent materials is crucial for informed decision-making in infrastructure planning, land-use management, environmental assessments, and geohazard mitigation. In the northern landscapes previously affected by glacial processes, these parent materials are predominantly Quaternary deposits. This study explored the potential of machine learning to expedite soil parent material mapping in Sweden. Two Extreme Gradient Boosting models were trained, one using terrain and hydrological indices derived from Light Detection and Ranging data, and the other incorporating additional ancillary map data. Both models were trained on 29,588 soil observations and evaluated against a separate hold-out set of 3500 observations. As a baseline, the existing most detailed maps achieved a Matthews Correlation Coefficient of 0.36. The Extreme Gradient Boosting models achieved higher MCC values of 0.45 and 0.56, respectively. To understand spatial variations in model performance, the second model was evaluated across 28 physiographic regions in Sweden. The results revealed that model performance varied across regions and deposit types, with till and peat exhibiting better performance than sorted sediments. These findings underscore the need for region-specific analyses to optimize the application of machine learning in digital soil mapping.

1. Introduction

Parent materials (PMs) are the initial state of the soil system (Jenny, 1994) and have a major influence on soil properties, which in turn affect nutrient availability, hydrology, and land stability (Anderson, 1988; Richter et al., 2019). Understanding the distribution of PMs is crucial for land-use planning, infrastructure construction, resource exploration, and geohazard recognition, as they carry significant environmental and societal impacts (Bernknopf et al., 1983; McMillan, 2002; Häggquist and Söderholm, 2015). PM can be broadly categorized as either primary in-situ or secondary transported material, such as alluvium, colluvium, aeolian, or glacial deposits (Gray and Murphy, 1999). In temperate regions, most soils have developed on soft rocks, or on unconsolidated sediments formed during the Quaternary period (the past 2.6 million years) through processes like erosion and deposition (Anderson, 1988). During glacial and postglacial times, these processes have created a mosaic of deposits at the surface that are different from the underlying bedrock geology (Lawley and Smith, 2008; Heung et al., 2014). The poor representation of the near-surface materials in existing geological maps often provide an erroneous view of soil PMs, further limiting their usefulness for soil modeling (Lawley and Smith, 2008; Lemercier et al., 2012). Producing PM maps (or often referred to as Quaternary Deposit (QD) maps in previously glaciated regions) is a labor-intensive, iterative process that often involves the collation and synthesis of diverse data sources. This often includes digitizing hand-drawn maps, compiling published and unpublished cartography or literature, and refining and updating maps by integrating data from new geophysical or geochemical investigations, with nationwide coverage typically achieved by amalgamating maps from different regions across the country (Weerts et al., 2005; Berg, 2009; Salazar Rincón et al., 2019).

The advent of Light Detection and Ranging (LiDAR) technology has revolutionized geomorphological and geological mapping across Scandinavia and beyond (Webster et al., 2006; Roering et al., 2013; Johnson et al., 2015; Ganerød et al., 2023), largely because it facilitated access to high-resolution Digital Elevation Models (DEMs), which have proven invaluable for identifying landscape features (Eilertsen et al., 2015;

* Corresponding author.
E-mail address: yiqi.lin@slu.se (Y. Lin).

https://doi.org/10.1016/j.geodrs.2024.e00905
Received 20 September 2024; Received in revised form 7 December 2024; Accepted 8 December 2024
Available online 10 December 2024

Peterson et al., 2017; Goodship and Alexanderson, 2020). Prior to the nationwide LiDAR scanning by the Swedish Land Survey (Lantmäteriet) in 2009, the methods for national scale QD mapping by the Geological Survey of Sweden (SGU) had remained unchanged for at least 15 years (Dowling et al., 2013). Such mapping relied heavily on ground investigations, supplemented by stereoscopic 3D viewing of aerial photographs and other thematic maps. Due to the time and effort required for manual mapping, priority has been given to areas of significant societal interest. As a result, while maps at a scale of 1:100,000 are available for large parts of Sweden, the highest-quality 1:25,000 scale maps are concentrated in the densely populated southern urban centers and agriculturally important regions (The Geological Survey of Sweden, 2024a). The vast northern inland areas, in contrast, rely on lower-resolution 1:1000,000 scale maps that depict generalized landforms (Fig. 1a) (The Geological Survey of Sweden, 2024b). Although QD maps at scales smaller than 1:100,000 are not intended for detailed planning and analysis, they are often the only resource available for national-scale mapping efforts (e.g., National Land Cover Map by The Swedish Environmental Protection Agency, 2020, Soil Moisture Map by Ågren et al., 2021). The lack of systematically available, detailed maps compromises the reliability of products derived from them - a problem that is not unique to Sweden (Lawley and Smith, 2008). Currently, at SGU, producing a 1:50,000 scale map for an area of 625 km^2 typically requires 250–350 h of work. This includes interpreting LiDAR and other remotely sensed data, conducting fieldwork, and compiling the maps. Given this approach, mapping the remaining areas of Sweden would take an estimated 50–100 years (personal communication, Cecilia Karlsson, Dec. 2024).

Similar to conventional soil mapping, in which soil surveyors or pedologists seek to establish conceptual relationships between soils and the landscape (Hudson, 1992), Digital Soil Mapping (DSM) techniques generalize and formalize soil classes or properties with spatially referenced environmental covariates for quantitative prediction (McBratney et al., 2003). Globally, DSM has transitioned from the academic domain to the operational stage (Arrouays et al., 2017; Zhang et al., 2017; Richer-de-forges et al., 2022). Advances in computing power and data storage, as well as the increasing availability of environmental datasets and regional soil databases, have fueled the rapid adoption of Machine Learning (ML) in DSM (Padarian et al., 2020; Wadoux et al., 2020). ML algorithms can handle complex relationships between large numbers of cross-correlated predictor variables and the target variable, a challenge for traditional geostatistical methods (Wadoux et al., 2020). Though DSM research covers a vast array of topics, its application to categorical mapping is limited (Wadoux et al., 2020). Recent developments have begun to expand this research area of multiclass mapping of soils over large areas (Ramcharan et al., 2018; Heung et al., 2022; Minarik et al., 2024, preprint). However, existing multiclass mapping studies of soil PMs are still often restricted to relatively small geographical extents (Lemercier et al., 2012; Latifovic et al., 2018), rely on limited field samples (Bonfatti et al., 2020; Prince et al., 2020; Krutskikh, 2022), or utilize synthetic training data (so-called 'pseudopoints') generated from polygon maps to improve spatial resolution through map disaggregation (Heung et al., 2014; Sorenson et al., 2023). In Sweden, DSM development has largely remained within the research realm, with studies typically conducted in specific regions (Söderström et al., 2016; Becher et al., 2019; Piikki and Söderström, 2019; Adler et al., 2022). Given the increasing demand for accurate and comprehensive QD maps in Sweden, especially for two-thirds of the country currently lacking detailed maps, there has been a growing interest in integrating DSM and ML techniques. In this context, our study is the first, to our knowledge, to explore the feasibility of generating wall-to-wall PM maps across a vast area (470,000 km^2) at a high resolution (4 m^2). Since most soil PMs in Sweden are QDs, we use the terms interchangeably to refer to the unconsolidated materials at the surface that are the foundation for eventual soil formation. However, we have retained the term 'QD maps' when directly referring to the official map products from the SGU.

In this study, we utilized data from 33,088 field observations obtained from extensive regional and national soil surveys for soil PM mapping in Sweden. Two separate Extreme Gradient Boosting (XGBoost) models were trained. The first model used exclusively terrain and hydrological indices derived from high-resolution airborne LiDAR data. A second model incorporating additional ancillary map data alongside the LiDAR-derived indices was trained and evaluated across Sweden's 28 physiographic regions. Our nationwide case study aimed to answer: (1) How do the ML-derived maps (using XGBoost) compare statistically to the existing QD maps? (2) Are certain PMs easier or more challenging to identify than others? (3) How do individual features impact the overall model performance, and the classification of individual PMs? and (4) Does the model performance exhibit spatial variation? Additionally, we provided a visual comparison between existing QD maps and the ML-derived maps, highlighting key differences and considerations for their application.

2. Material and methods

2.1. Study area

The study area spans most of Sweden, excluding the data-scarce mountain regions in the northwest (Fig. 1). Situated between 55° N and 70° N and 11° E and 25° E, Sweden covers an area of ca. 470,000 km^2. The country exhibits a diverse geomorphology, ranging from mountainous terrain in the northwest to lowland plains in the south. Located within the boreal and nemoboreal zone of northern Europe, Sweden's landscape is predominantly forested (68 %), followed by open mires and other open land uses (22 %) and arable land (7 %) (Statistics Sweden, 2019). Exposed bedrock constitutes a minor portion of the country's surface, while large parts of the bedrock are covered by Quaternary unconsolidated glacial deposits (glaciofluvium and till) and postglacial deposits (clay, silt, and peat), formed and shaped by glaciers, water, and to a lesser extent, wind (Donner and Donner, 2005). During the post-glacial times, the retreat of the glacier border triggered a period of rapid isostatic rebound and land uplift due to the release of pressure from the overlying ice cap (Karlsson et al., 2014). The central lowlands and areas around the coast that were submerged under the sea after glaciation are now partially covered by glacial and post-glacial clays (Agrell, 1979). With the land uplift, wave actions reworked till and glaciofluvial deposits in these areas to form littoral sand and gravel (Agrell, 1979) (Fig. 1b). The warmer humid climate, combined with a high groundwater table, created favorable conditions for peat formation (Franzén et al., 2012; Morris et al., 2018; Piilo et al., 2020). The country is divided into 29 distinct physiographic regions based on climatic, topographical, biological, and geomorphological factors (Helmfrid, 1996) (Fig. 1c).

2.2. Field data

For model training, we utilized field sampling data from (1) the Swedish Forest Soil Inventory (SFSI) (Fig. 1d), and (2) the Swedish Agricultural Soil Inventories (SASI) (Fig. 1e).

2.2.1. Swedish forest soil inventory (SFSI)

The Swedish Forest Soil Inventory (SFSI) consists of 19,650 georeferenced soil pits across 5 survey regions, excluding urban areas, cultivated land, water bodies, and high mountain regions (Fig. 1d). We utilized data collected during the sampling round from 2003 to 2012. PM and grain size were determined with a probe to collect soil samples from a minimum of 20 cm beneath the lower boundary of the humus layer. The pits were georeferenced with a GPS measurement error of up to 10 m. The SFSI classifies soil based on five PMs (well-sorted sediments, poorly sorted sediments, till, bedrock outcrops, and peat) and eight texture classes (cobble and stone (20–200 mm), gravel (2–20 mm), coarse-grained sand (0.6–2 mm), medium-grained sand (0.2–0.6 mm),

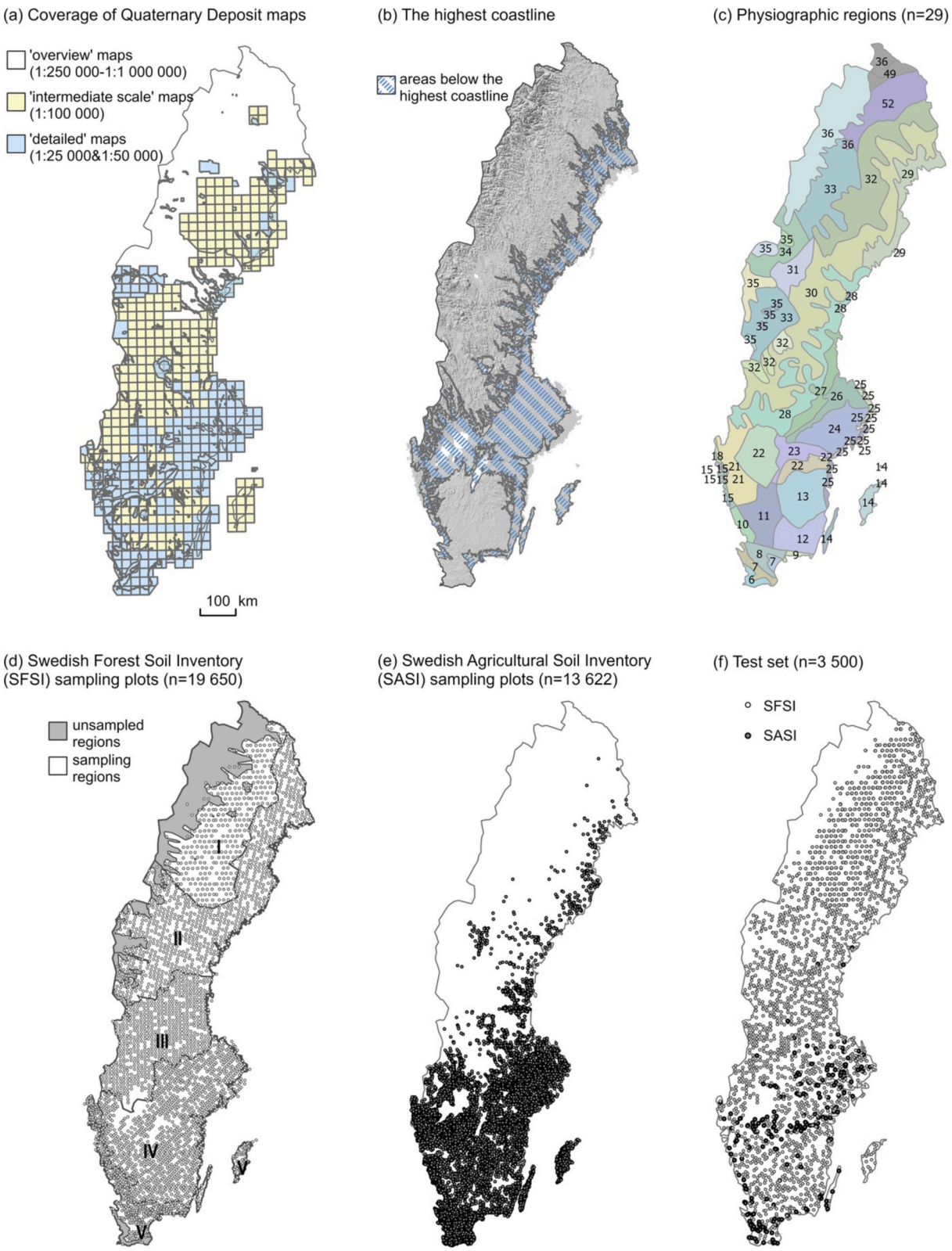

Fig. 1. Spatial data of Sweden. (a) Coverage of the Quaternary deposit (QD) maps by the Geological Survey of Sweden as of spring 2024, reclassified into three categories (source: the Geological Survey of Sweden). (b) The highest coastline is shown on a background map featuring a Digital Elevation Model (DEM). The blue hatched areas were submerged beneath the sea before land uplift following deglaciation (source: Geological Survey of Sweden). (c) Sweden is divided into 29 distinct physiographic regions based on geology, topography, and biology etc. See Fig. 5 for detailed legends (source: the National Atlas of Sweden). (d) Field sampling plots from the Swedish Forest Soil Inventory (SFSI). Sampling density increases from I to V. (e) Field sampling plots from the Swedish Agricultural Soil Inventory (SASI). Higher sampling density in the southern agricultural regions. (f) Distribution of the test set, constructed from (d) and (e).

fine-grained sand (0.06–0.2 mm), coarse silt (0.02–0.06 mm), fine silt (0.002–0.02 mm), clay (< 0.002 mm)) (The Swedish National Forest Inventory, 2021). Readers can refer to the SFSI sampling protocol for detailed instructions on PM and texture classification (The Swedish National Forest Inventory, 2021).

2.2.2. Swedish agricultural soil inventories (SASI)

Due to their similar characteristics, we combined topsoil samples (0–20 cm) from two national agricultural soil sampling campaigns: 12,599 topsoil samples (2011−2012) were collected by the Swedish Board of Agriculture (Jordbruksverket) from a more or less regular grid with a density of approximately 1 sample km^{-2} (Piikki and Söderström, 2019), and 5142 topsoil samples (1988–2017) collected by the Swedish Environmental Protection Agency (Naturvårdsverket) (Fig. 1e). Agricultural soil samples are concentrated in the south, reflecting the higher prevalence of agricultural land in that region. The determination of surface deposit types in our investigation was based on the percentage of sand, clay, and silt content. We classified fine sediments as those with a majority grain size $\leq$0.2 mm and coarse sediments as those with a majority grain size >0.2 mm. In total, the SASI dataset comprises 13,622 samples after data cleaning.

2.3. Data harmonization and partition

There are discrepancies in data collection methods and classification schemes between QD maps and field surveys. The SFSI and the original QD maps represent soil PMs at more comparable depths (SFSI at least 20 cm below the humus layer, QD maps 50 cm below the surface), while SASI represents topsoil up to 20 cm below the surface. To facilitate model training and comparison with the existing maps, a tailored harmonization process was devised collaboratively with the experts from the SGU where all 48 categories were reclassified into 7 more general soil PM classes: till, rock outcrops, peat, and two types of sorted sediments (coarse (fine sand-gravel) and fine (clay-silt)) from forest and agriculture land use, respectively. We defined sorted sediments as primarily transported and deposited by water, with a potential minor wind contribution. Fine sediments (clay-silt) were defined as having a grain size less than or equal to 0.2 mm, while coarse sediments (fine sand-gravel) were larger than 0.2 mm. Till, in contrast, was glacially deposited and generally unsorted. In Sweden, definitions of peat vary (at least 20 % organic material and minimum thickness of 30 cm, 40 cm, or 50 cm). In this study, we adopted the 50 cm threshold as defined by SGU (Ågren et al., 2022).

We created a test set with uniform sampling density across our study area (Fig. 1f), following simple random sampling principles (Brus et al., 2011) to generate a random subset from our original samples. This resulted in a test set totaling 3500 points (0.02 samples km^{-2}). The remaining 29,588 points were used for model training (0.06 samples km^{-2}). Further details regarding the harmonization procedure were provided in the Supplementary Material Table. A.1, and sample counts for all final classes in the training and evaluation sets were provided in the Supplementary Material Table. A.2.

2.4. Environmental covariates

2.4.1. The quaternary deposit (QD) maps from the Geological Survey of Sweden (SGU)

The QD maps from SGU provide a foundation for understanding Sweden's geology, surface deposit formation, and grain size composition (Karlsson et al., 2021). These maps depict the base layer (geology), the distribution of QDs 50 cm below the ground surface, and in some cases, thin/discontinuous surface layers between 0 and 50 cm at the ground surface. Specific landforms such as hummocky moraine and sand dunes are detailed with additional line and point layers (Karlsson et al., 2021). For this study, we classified the original QD map types into three categories based on their scale and cartographic methods. 'Detailed maps' (1:25,000 & 1:50,000) cover approximately 35.8 % of Sweden, primarily concentrated in southern urban centers and regions with agricultural importance (Fig. 1a). The 1:25,000 scale maps were created through a combination of manual interpretation of LiDAR DEMs and extensive field surveys. They are often an update from older 1: 50,000 maps. The 1: 50,000 scale maps were produced through extensive field surveys with manual interpretation of aerial photographs, topographic maps, and economic maps. 'Intermediate scaled maps' (1:100,000), covering 41.7 % of the country, were created by interpreting aerial photos and validated with less extensive field surveys. The remaining 22.5 % of the country, primarily in the northern inland, mostly rely on the 'overview maps' (between 1:250,000 and 1:1000,000) created partly based on aerial photograph interpretation with less intensive fieldwork, or digitizing analog, hard-copy maps(The Geological Survey of Sweden, 2018; 2024a; b; c; d). A nationwide QD map was provided in Supplementary Material Fig. A.1. This map was created by combining the highest-quality maps available for each region. For visualization on static media, we chose the version with simplified classes for readability without zooming possibilities. Readers can explore detailed, interactive maps on SGU's web map viewer at: https://apps.sgu.se/kartvisare/kartvisare-jordarter-25-100.html (for 'detailed' maps), or https://apps.sgu.se/kartvisare/kartvisare-jordarter-1-miljon.html (for 'overview' maps).

2.4.2. Environmental features for machine learning models

Two main sources of environmental features were used to train the ML models. Terrain and hydrological indices were derived from the original 2-m LiDAR DEM (Table 1). These features captured landforms and hydrological characteristics at various scales:

- 9 indices were derived directly from the high-resolution 2-m DEM for fine-scale details.
- To encompass larger landscape features, we resampled the 2 m DEM to 20 m and 50 m using the bilinear interpolation method to facilitate the calculation of an additional 13 and 4 indices, respectively. For detailed descriptions of these indices see the WhiteboxTools User Manual (Lindsay, 2024).

We further integrated ancillary data from existing maps and satellite imagery, including:

- Normalized Difference Vegetation Index (NDVI): Using cloud-free (<20 % cover) Sentinel-2 satellite imagery, we computed the median NDVI for the growing seasons (June 1 to September 30) from 2017 to 2023.
- Original Quaternary Deposit (QD) Map (The Geological Survey of Sweden, 2018; 2024a; b; c; d): This map was compiled from the best available QD maps in 2020 (scales vary from 1:25,000 to 1:1000, 000).
- Depth to Bedrock Map (Daniels and Thunholm, 2014): This map interpolates data from sources such as borehole drilling records, hydrogeological explorations, and seismic profiles. It uses the QD map as an input (assuming 0 m for rock outcrops).
- National Land Cover Map (The Swedish Environmental Protection Agency, 2020): The 2018 National Land Cover Map incorporates data from 41 sources, including the QD map, LiDAR DEM, Depth to Bedrock map, Sentinel-2 imagery, and other geospatial layers, resulting in a 10-m resolution map with 25 land cover classes (Minimum Mapping Unit (MMU): 0.01 ha).
- Distance to Highest Coastline (The Geological Survey of Sweden, 2015): This feature identifies the distance to a critical reference point – the highest coastline which indicates the maximum elevation reached by the sea after deglaciation and land rebound (Fig. 1b). Areas above this line are dominated by glacial deposits and peat, while areas below have more diverse water-deposited sediments. This feature is derived from data points in SGU and Geological Survey of Finland (GTK) databases.

Table 1
Feature layers used XGBoost model training. Each entry details the name, scale, specific settings in processing if applicable (such as search area or filter kernel size), data median, and range. All layers were resampled to 2 m resolution. Features indicated with an asterisk (*) were incorporated in the production of the National Land Cover Map. (a) LiDAR-derived indices. (b) Ancillary map data.

(a)

LiDAR derived digital terrain indices

Feature	Scale /Resolution	Specific Settings	Raster value median (range) /Number of classes	*Source*
Digital Elevation Model (DEM)*	2 m		110.94 (−2.07–863.65)	(The Swedish Land Survey, 2022)
Elevation above stream from a 1 ha stream network	2 m		2.0 (0.0–154.0)	(Lindsay, 2024)
Elevation above stream from a 10-ha stream network	2 m		4.0 (0.0–246.0)	Ibid.
Downslope index with 2 m drop	2 m		124.45 (2.0–31,250.0)	Ibid.
Downslope index with 2 m drop	20 m		0.07 (0.0–176.6)	Ibid.
Circular variance of aspect	2 m	3	0.05 (0.0–0.99)	Ibid.
Circular variance of aspect	20 m	5	0.21 (0.0–0.99)	Ibid.
Circular variance of aspect	50 m	11	0.28 (0.0–0.99)	Ibid.
Standard deviation of Slope	2 m	3	0.67 (0.02–21.93)	Ibid.
Deviation from mean elevation	2 m	7	−0.02 (−3.09–3.58)	Ibid.
Terrain ruggedness index	2 m		0.1 (0.0–4.14)	Ibid.
Average normal vector angular deviation	20 m	15	2.40 (0.11–56.0)	Ibid.
Multi-Scale roughness magnitude	2 m	Min_scale = 1, max_scale = 10, step = 2	1.98 (0.2–45.58)	Ibid.
Maximum Elevation deviation	2 m	Min_scale = 50, max_scale = 500, step = 50	−0.37 (−4.49–8.15)	Ibid.
Maximum Elevation deviation	20 m	Min_scale = 20, max_scale = 200, step = 11	0.0 (−5.55–3.42)	Ibid.
Maximum Elevation deviation	50 m	Min_scale = 50, max_scale = 500, step = 50	−0.49 (−4.92–7.8)	Ibid.
Max downslope elevation change	20 m		1.36 (0.21–3975.46)	Ibid.
Topographic Wetness Index	20 m		7.32 (−1.49–21.24)	Ibid.
Slope	20 m	20	2.58 (0.01–89.35)	Ibid.
Slope	50 m	50	1.53 (0.01–40.35)	Ibid.
Relative topographic positions	20 m	x = 11, y = 11	0.04 (−0.99–1.0)	Ibid.
Maximal curvature 20 m	20 m		0.0 (−0.02–0.19)	Ibid.
Maximal curvature 50 m	50 m		0.0 (−0.0–0.08)	Ibid.
Minimal curvature 20 m	20 m		−0.0 (−0.27–0.04)	Ibid.
Directional relief	20 m		278.43 (−44,738,810.1–1359.53)	Ibid.
Geomorphons	20 m	50	9 classes	Ibid.
Profile curvature	20 m		(−1.2–0.14)	Ibid.

(b)

Feature	Scale /Resolution	Specific Settings	Raster value median (range) /Number of classes	*Source*
Ancillary Map Data				
SGU Quaternary Deposit Map base layer up to 0.5 m below surface*	1:25,000 to 1: 1000,000		12 classes	(Karlsson et al., 2021)
National land cover map	10 m		23 classes	(The Swedish Environmental Protection Agency, 2020)
Age from deglaciation	?		11.51 (10.0–17.28)	(Hughes et al., 2016)
Distance to the highest coastline	1:100,000–1:200000		8.0 (0.0–255.0)	(The Geological Survey of Sweden, 2015)
Depth to bedrock*	10 m		7.43 (0–179.64)	(The Geological Survey of Sweden, 2023)
Normalized difference vegetation index (NDVI) (Sentinel 2) *	400 m		0.41 (−0.04–0.91)	
Coordinates				
Easting	2 m		568,679 (280795–913,007)	
Northing	2 m		6,920,018 (6141258–7,608,074)	

- Age from Deglaciation: Derived from DATED-1 time-slice reconstruction of the evolution of the extent of the Eurasian ice sheets 25–10 ka (Hughes et al., 2016).

All covariate data layers were resampled to a common resolution (2 m) and aligned to the national projection system (SWEREF99 TM). We utilized established open-source geospatial libraries for preprocessing data. Terrain and hydrological indices were calculated using WhiteboxTools (v2.3.0) (Lindsay, 2024). Other geospatial data manipulation, including resampling and raster value extraction, was facilitated by GDAL/OGR (v3.9.1) (GDAL/OGR contributors 2024) and Rasterio (v1.3.10) (Gillies, 2019) Python package. Sentinel-2 satellite imagery was accessed and processed through Google Earth Engine (GEE) (Gorelick et al., 2017) and its Python API geemap (v0.33.1) (Wu, 2020).

2.5. Extreme gradient boosting (XGBoost) model training

The Extreme Gradient Boosting (XGBoost) algorithm was employed

due to its efficiency in handling large datasets through optimized data structures and parallelization techniques (Chen and Guestrin, 2016). It is a tree ensemble model, but unlike Random Forest, which builds trees independently and derives the final prediction by majority voting (classification) or averaging (regression), XGBoost builds trees sequentially and corrects errors from the previous ones using gradient updates. It is less prone to overfitting due to built-in L1 and L2 regularization. For classification problems, the final prediction of XGBoost is assigned to the class with the highest probability. Its robustness has been demonstrated in national-scale applications in Sweden (Ågren et al., 2021; Ågren and Lin, 2024).

In this study, two XGBoost models were trained using the Python libraries scikit-learn (v1.5.1) (Pedregosa et al., 2011) and XGBoost (v2.1.1) (Chen and Guestrin, 2016). The first model utilized only LiDAR-derived indices as input features. The second model incorporated the same LiDAR features and additional maps (Table 1). To optimize hyperparameters, we employed the Tree-structured Parzen Estimator (TPE) sampler (Watanabe, 2023) implemented in Optuna (v3.6.1) (Akiba et al., 2019). The objective function was to maximize the mean Matthews Correlation Coefficient (MCC) (Matthews, 1975) across five-fold cross-validation on the training set ($n = 29{,}588$) over 100 trials. Each XGBoost model was trained with 100 fixed random states to ensure deterministic behavior and allow for a fair comparison of their performance. Throughout this study, all computations were performed on a Linux system (Ubuntu 22.04.2) with an AMD Ryzen ThreadRipper 3990× processor (64 cores, 2.9 GHz, 256 MB cache) and 256 GB of DDR4 RAM.

2.6. Model evaluation

2.6.1. Evaluation metrics

We evaluated model performance on the unseen hold-out set ($n = 3500$) using the following metrics: MCC (Matthews, 1975) for overall performance, and F1 score (harmonic mean of precision and recall) for class-specific performance. The precision, recall, and F1 scores of the best-performing XGBoost models (LiDAR-only and all features) based on MCC from 100 iterations were reported. Additionally, SHAP values were employed to identify the key features using the Python package SHAP (v 0.39.0) (Lundberg and Lee, 2017). A global measure was calculated by taking the mean of the absolute SHAP value for each feature across all instances in the hold-out test set. We computed MCC values across physiographic regions using the test set for the best-performing XGBoost model (all features). Only physiographic regions with a minimum of 80 field observations were selected to ensure sufficient data for reliable metric calculation. This approach provides a more nuanced understanding of the spatial variation in model performance and its applicability, particularly in regions lacking detailed QD map coverage.

2.6.2. Visual comparison of maps

To facilitate visual comparison, we focused on a peat-rich region in northern Sweden (64°23′N, 19°78′E). This area, well-known to the authors through decades of extensive research and established local knowledge (Laudon et al., 2013, 2021), provides a reliable basis for ground-truthing. Moreover, a high-quality QD map (1:25,000) produced by the SGU was available for this area. This map was created through extensive field investigations and the use of high-density LiDAR data (20 points m^{-2}), significantly exceeding the national average of 1–2 points m^{-2}. Four spatial representations of peat were presented: 1) an existing 'overview' QD map (1:1000,000), 2) a high-quality 'detailed' QD map (1:25,000), 3) an XGBoost (LiDAR only)-inferred map and 4) an XGBoost (all features)-inferred map. By displaying the 'overview' QD map, we aimed to exemplify the challenges faced by areas lacking high-resolution 'detailed' maps.

3. Results and discussion

3.1. Evaluation of existing QD maps and XGBoost model performance

To establish a baseline for assessing the performance of the XGBoost models, we evaluated the existing QD maps across scales using the hold-out test set (n = 3500) (Fig. 1f). On a country level, the 'overview' maps (1:250,000–1:1000,000) achieved a low level of agreement with the field data with an MCC of 0.18, followed by 'intermediate scale' maps (1:100,000) at 0.19. The highest agreement with the field plots was found with the 'detailed' maps (1:25,000–1:50,000) at an MCC of 0.36 (Table 2). Knight and Lunetta (2003) found a positive correlation between Minimum Mapping Units (MMU) size and accuracy metrics, up to the threshold of 6.4 ha, beyond which improvements plateaued. In contrast, our study revealed an opposite trend, with the evaluation metric MCC improving as MMU size decreased. However, a similar plateau effect was observed between 'intermediate-scale' maps (MMU: 2500–10,000 m^2) and 'overview' maps (MMU: 40000–1000,000 m^2) (Table 2) as the MMU sizes reached a comparable threshold to that identified in the aforementioned study (64,000 m^2). The trend in our study could be due to the fundamental differences in map-making methods and the classification details between different map types, as opposed to resampling raster maps to different MMUs in the study by Knight and Lunetta (2003). The 'detailed' maps were produced using rigorous methods, including interpreting LiDAR DEM and extensive field validation, enabled the identification of a more comprehensive range of surface deposit types. With smaller MMU of 625 m^2 for 1: 25,000 and 2500 m^2 for 1: 50,000 scales, the 'detailed' maps achieved average location errors (location of delineation between different QDs) between 25 and 100 m (Table 2). In contrast, 'overview' maps were created with a fixed display scale of 1:250,000 to 1:1000,000 where only large-scale QDs were identified. Their digitization was based on broader assumptions and generalizations, resulting in larger location errors (200 to 1000 m) (Table 2).

The XGBoost (LiDAR only) model achieved a mean MCC of 0.45 (Table 2), surpassing the MCC of 0.36 obtained by the 'detailed' maps. However, this result pertains to our 7-class ML model, which lacks the level of detail of the original 48-class QD maps (Supplementary Material Table. A.1). Although the relatively low MCC values of the QD maps raised concerns about potential error propagation into the ML process, the inclusion of them improved model performance, with XGBoost (all features) achieving an MCC of 0.56 (Table 2). This improvement can be attributed to the pedological expertise and insights captured in the original maps, in combination with the ability of ML techniques to filter out noise and capture underlying soil-environmental relationships (Teng et al., 2018; Liu et al., 2022). Another possible explanation could lie in the support (n), defined by volume, size, shape, and spatial orientation

Table 2
Evaluation of Quaternary Deposit Maps using Matthews Correlation Coefficient (MCC). Note that the number of data points within each map type may vary. A detailed breakdown of the precision, recall, F1 scores, and support (n) was provided in Supplementary Material Table. A.3.

Map type (scale)	MCC	n	Average location error (Karlsson et al., 2021)	Minimum mapping unit
'Overview' maps (1: 250,000–1: 1000,000)	0.18	934	200–1000 m	40,000–1000,000 m^2
'Intermediate scale' maps (1: 100,000)	0.19	1522	100–200 m	2500–10,000 m^2
'Detailed' maps (1: 25,000–1: 50,000)	0.36	987	25–100 m	625 & 2500 m^2
XGBoost (LiDAR only) (2 m)	0.45	3500	10 m	4 m^2
XGBoost (all features) (2 m)	0.56	3500	10–1000 m	4 m^2

(Gotway and Young, 2002). Point-based support usually presents the worst-case scenario, potentially leading to an underestimation of the true accuracy (Bishop et al., 2015). The actual quality of the QD maps might exceed the level indicated by this point-based evaluation. Nevertheless, spatially explicit comparisons between raster and vector datasets are challenging due to spatial and categorical mismatches (Wulder et al., 2006). Additionally, the GPS positioning errors of up to 10 m of the field samples can also undermine the reliability of the evaluation. Despite these uncertainties, the higher MCCs for the XGBoost models indicate the feasibility of using ML to automatically generate high-resolution future maps based on laser data and/or ancillary map data.

3.2. Visual comparison of maps

Waterbody polygons from the Swedish Property map (1:12,500) retrieved from the Swedish Land Survey were overlaid on all maps to aid visual interpretation. The limitation of using 'overview' maps for

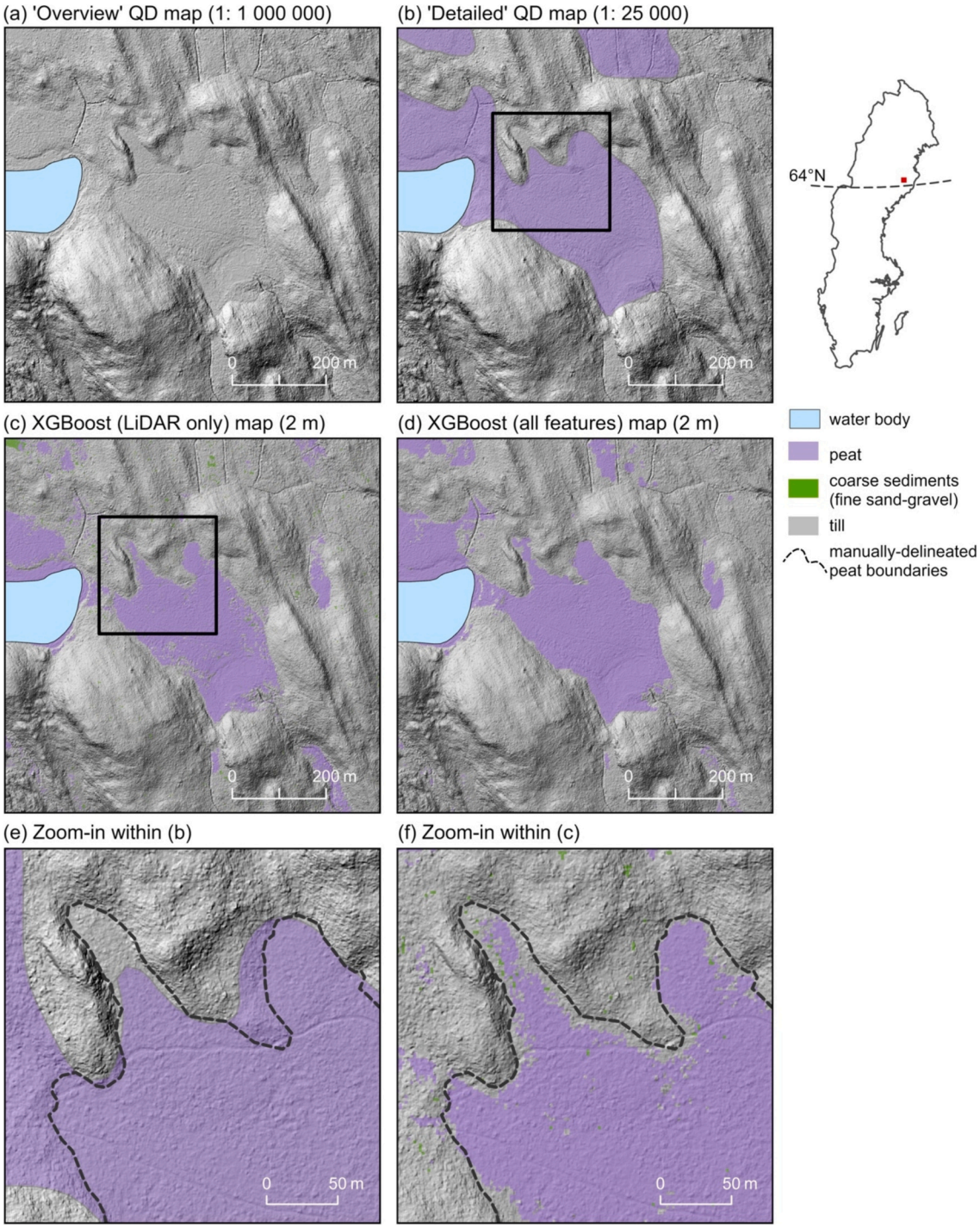

Fig. 2. Visual comparison of peat deposit distributions. (a) Quaternary Deposit (QD) map (1:1000,000) exemplifies the limitations of the 'overview' maps. (b) 'Detailed' QD map (1:25,000). (c) XGB (LiDAR only)-inferred map (2 m) and (d) XGB (all features)-inferred map (2 m). (e) and (f) zoom in to areas within panels (b) and (c), providing a closer look at the delineation of peat and till boundaries. The dashed lines in figures (e) and (f) indicate our interpreted border between till and peat based on the digital elevation model (DEM) and field visits.

detailed analysis is evident in Fig. 2a, where the peatland area was entirely omitted due to polygon map generalization. This process, commonly employed to enhance polygon map legibility at small scales, involves the elimination of certain small polygon features, smoothing of contours, and aggregation of closely spaced features (Smirnoff et al., 2012; Sayidov et al., 2020). While 'overview' QD maps (scales <1:100,000) are acceptable for national-level visualization, their use in other contexts such as GIS analyses, detailed planning, and decision-making requires caution (The Geological Survey of Sweden, 2024b). Conversely, the 'detailed' QD map (Fig. 2b), the XGBoost (LiDAR only) (Fig. 2c), and the XGBoost (all features) (Fig. 2d) exhibit similar spatial patterns for the peat extent. However, discrepancies were apparent when zooming in on specific areas within the 'detailed' QD map and the XGBoost (LiDAR only) map (Fig. 2e & f). The high-resolution raster maps also exhibit uncertainties, as demonstrated by the green pixels (coarse sorted sediments) in the XGBoost (LiDAR only) maps (Fig. 2c & f), known as the 'salt-and-pepper' effect (Blaschke et al., 2000, 2014; Whiteside et al., 2011). The isolated pixels are likely artifacts, as most landscape features need to be represented by areas larger than the size of an individual pixel (Whiteside et al., 2011). Various post-processing techniques to filter out noise could be applied to mitigate the visual clutter arising from undergeneralization in Fig. 2c-f. The harmonization process integrating materials from postglacial, glacial, and glaciofluvial processes (Supplementary Material Table A.1) further complicates the distinction between noise and actual landscape features based solely on model output. This also highlights the importance of expert knowledge when implementing DSM with ML during the model training process and for interpreting model outputs (Rossiter et al., 2022). The XGBoost (all features) map benefited from the high spatial resolution of a raster map, allowing for a detailed depiction of small landscape features, while incorporating existing QD maps during training prevented the generation of isolated pixels as observed in the XGBoost (LiDAR only) model. For practical purposes, the XGBoost (all features) might be the best model for application.

3.3. Predictive capability for different soil parent material classes

Our training data originates from two landscapes: forest (SFSI) and agricultural (SASI). To aid the visualization in Fig. 3, shapes were employed to represent 'detailed' QD maps (triangles), XGBoost (LiDAR-only) model (crosses), and XGBoost (all-features) model (circles). We used marker styles to differentiate PM types, with full markers representing PMs in forest land use, and half markers for those occurred in agricultural land use. Further color coding was applied (Fig. 3). Both XGBoost models excelled at classifying till, the dominant soil PM, achieving F1 scores of 0.82 (all features) and 0.80 (LiDAR only), while the 'detailed' QD maps achieved an F1 score of 0.60. This could be due to the slight discrepancies in the definition of till in the original QD maps and field sampling, where the QD maps can contain well-sorted sediments whereas field sampling defines till strictly as unsorted glacial deposits. XGBoost also demonstrated an improvement in peat classification, achieving F1 scores of 0.76 (all features) and 0.65 (LiDAR only) compared to 0.30 of 'detailed' QD maps (Fig. 3). This aligns with previous peat-specific DSM studies globally and in Sweden (Artz et al., 2019; DeLancey et al., 2019; Karlson et al., 2019; O'Leary et al., 2022; Rimondini et al., 2023). The multiclass nature of the XGBoost models offers more efficiency compared to managing multiple single-class models. The high-resolution models also have the potential to identify smaller or otherwise unmapped peatlands, which is valuable for peatland management and conservation efforts (Ågren et al., 2022).

Both XGBoost models struggled to differentiate between coarse and fine forest sorted sediments (Fig. 3), an issue noted in other multiclass DSM studies (Mulder et al., 2016; Ramcharan et al., 2018). Chen et al. (2022) highlighted the challenges in predicting coarse sediments due to their high spatial variability and recommended increasing field sampling as a potential strategy. McBratney et al. (2003) proposed

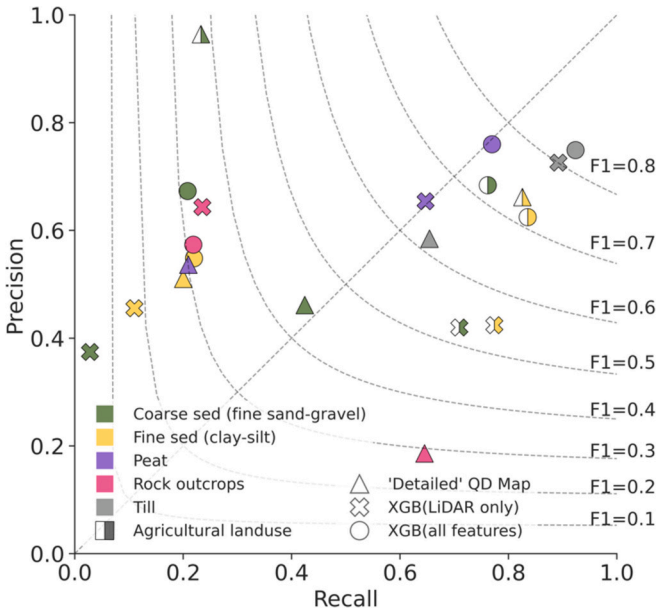

Fig. 3. The figure illustrates the performance of the 'detailed' Quaternary Deposit (QD) maps (triangles), XGBoost model trained with only LiDAR (crosses), and XGBoost model trained with all features (circles) for identifying different soil parent materials (PMs). Isolines represent F1 scores, the harmonic mean of precision (correctly identified) and recall (identification completeness). Half-filled markers denote PMs on agricultural land, while full markers represent forest land. Points under the 1:1 line are over-predicted and points above the line are under-predicted.

simplifying legends, reducing resolution, or conducting targeted sampling in regions with poor predictability. Similarly, Loiseau et al. (2021) recommended a threshold sampling density of about 1 sample 2 km^{-2} for clay, silt, and sand contents to avoid a substantial decrease in performance accuracy. Coarse and fine sorted sediments on agricultural lands, formed through simpler water deposition processes, had significantly more training samples (Supplementary Material Table. A.3). These soil PM types were effectively classified by XGBoost (all features), with F1 scores exceeding 0.72, which may suggest that increasing sampling density enhances model performance.

Rock outcrops on 'detailed' QD maps had high recall (0.63) but low precision (0.19) (Fig. 3, Supplementary Material Table. A.3), indicating frequent misclassification of other QDs as rock outcrops. This may be a result from the over-exaggeration of rock outcrop boundaries on polygon maps. In contrast, both XGBoost models demonstrated higher precision but lower recall, suggesting that while they often miss true rock outcrops, those identified as rock outcrops are typically accurate. This may be attributed to the limited availability of rock outcrop training samples (Supplementary Material Table A.2), as similarly observed with sorted sediments in forest landscapes. Additionally, the varying appearance of rock outcrops on LiDAR DEM could have presented further challenges. Several studies have highlighted the potential benefits of data resampling techniques, such as SMOTE (Synthetic Minority Oversampling Technique), to address imbalanced class distributions (Sharififar et al., 2019; Mirzaei et al., 2024). Thus, exploring class balancing techniques could be a promising strategy for enhancing model performance for minority classes.

3.4. Feature importance and the impact of LiDAR indices

SHAP values provided insights into the relative contributions of different features in the predictions of both XGBoost models (Fig. 4, showing only the top 15 most important features). The length of each bar in the SHAP plot represents the feature's overall importance as

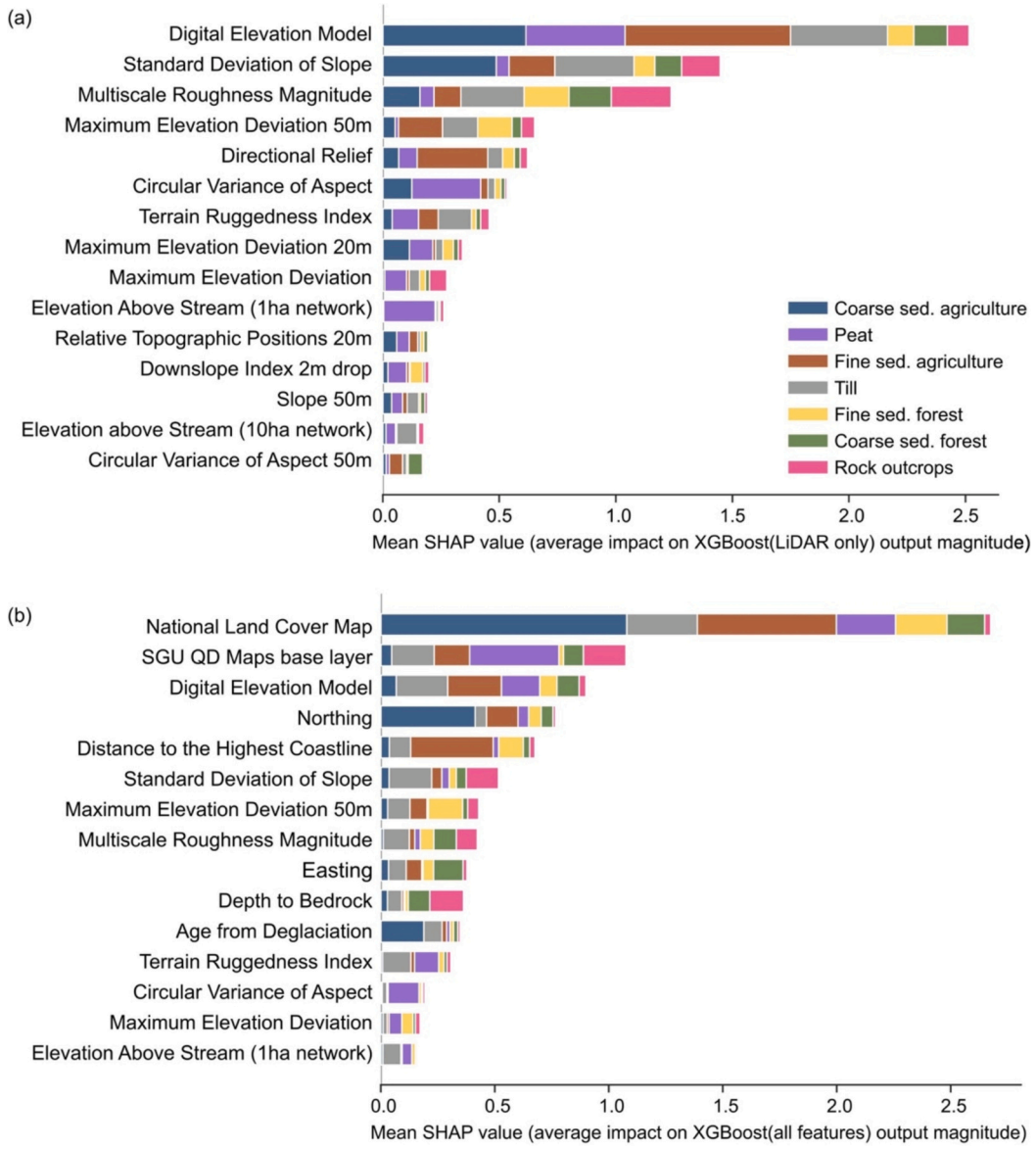

Fig. 4. SHAP (SHapley Additive exPlanations) values represent the relative importance of each feature in the XGBoost models' prediction of soil parent materials (PMs), with higher values indicating greater contribution. (a) SHAP summary plot for XGBoost (LiDAR only). (b) SHAP summary plot for XGBoost (all features).

determined by the model. In the XGBoost (LiDAR only) model, the original 2 m DEM was the most critical feature, particularly for identifying peat, till, and agricultural sediments (Fig. 4a). This finding underscores the capability of LiDAR in capturing high-resolution surface characteristics crucial for these classifications. The Circular Variation of Aspect (measures surface shape complexity, or texture) and Elevation above Stream (represents the relative vertical distance to drainage, measured along the downslope flow path) from a 1 ha stream network also contributed significantly to the prediction of peat (Fig. 4a). The characteristic flatness and poor drainage of peatlands were likely reflected in these indices, while a low flow accumulation threshold (1 ha) for Elevation above Stream captured areas with poor local drainage, which are favorable for peat development (Ehnvall et al., 2023). Similarly, Heung et al. (2014) found that aspect, distance to nearest stream, convergence index, and distance to nearest river to be the most important features for predicting parent material in the Canadian west coast, while slope, plan curvature, and profile curvature were the least important.

The most important feature for XGBoost (all features) to predict surface deposits was the National Land Cover Map (Fig. 4b). This map was crucial for identifying most surface deposit types, especially agricultural sorted sediments, likely due to the 'arable land' category within the map and the overrepresentation training data from the SASI dataset. For peat delineation, the original QD map was the most important (Fig. 4b), replacing Elevation above Stream as a key feature. The Distance to the Highest Coastline was crucial for identifying agricultural fine sediments, while Northing (latitude) and Age from Deglaciation significantly impacted the delineation of agricultural coarse sediments. These indices reflect the glacial history and post-glacial land rebound in the Bothnian Bay region (Stroeven et al., 2016; Nordman et al., 2020), which directly influenced the spatial distribution of sorted sediments. Rock outcrops were primarily identified based on Depth to Bedrock, which contains similar information as the original QD maps. The importance of Multiscale Roughness Magnitude diminished relative to other LiDAR-derived features (Fig. 4a) when additional ancillary map data were incorporated (Fig. 4b). This suggests that information from the QD Maps and Depth to Bedrock might have assumed the role previously played by Multiscale Roughness Magnitude in identifying rock outcrops for the XGBoost (LiDAR only) model.

Overall, conventional maps were more important than LiDAR-

derived indices in the XGBoost (all features) model. The inclusion of some conventional maps in the production of the National Land Cover map (marked with * in Table 1) may confound the interpretation of feature importance. Class imbalance within the training dataset can influence feature importance (Mirzaei et al., 2024). It is likely that applying resampling techniques to our training set, as discussed in Section 3.3, would have altered the feature importance rankings. Recent DSM studies found that though in general finer resolutions yield better performance in heterogeneous landscapes, and coarser resolution data is more effective in homogeneous landscapes; their effectiveness is highly dependent on the specific soil class or properties of interest, local environmental characteristics, and the geographical extent under consideration (Cavazzi et al., 2013; Larson et al., 2022; Piedallu et al., 2022). We calculated terrain and hydrological indices at different resolutions, examining the impact of scale on model performance, however, is beyond the scope of this study. A study conducted in eastern Canada using only four LiDAR-derived terrain indices achieved high overall performance in mapping parent materials, with Cohen's Kappa of 0.76 (Prince et al., 2020). Considering the recent trend towards utilizing high-dimensional and high-resolution data in DSM studies, it is imperative to conduct a meticulous feature selection process to ensure scale appropriateness and minimize model complexity.

3.5. Model performance across physiographic regions

This spatial analysis was only applied to XGBoost (all features) model due to its higher overall MCC. A spatial trend across Sweden's physiographic regions could be observed, where the northern inland regions (30–34), dominated by till and peat, generally achieved slightly higher MCCs compared to southern and coastal regions (11–29) (Fig. 5). As an exception, region 24 exhibited good model performance, which could be due to the high-quality QD map for this area. Till and fine-grained agricultural sediments were consistently overpredicted across the country (Fig. 5), likely owing to their overrepresentation in the training dataset (Supplementary Material Table A.2). In contrast, forest sediments were generally underpredicted. Peat and agricultural coarse sediments demonstrated more variable performance: peat was typically underpredicted in central Sweden (regions 24–26) but overpredicted in the north and south, while agricultural coarse sediments were overpredicted in the far south (regions 11–21) and underpredicted in south-central Sweden (regions 22–28). A closer examination of the class-wise training data distribution by region is necessary to determine if these patterns reflect data availability. Given that the model performs better in the northern inland areas, where only 'overview' and 'intermediate-scale' QD maps are available (Fig. 1a), there is great potential for using

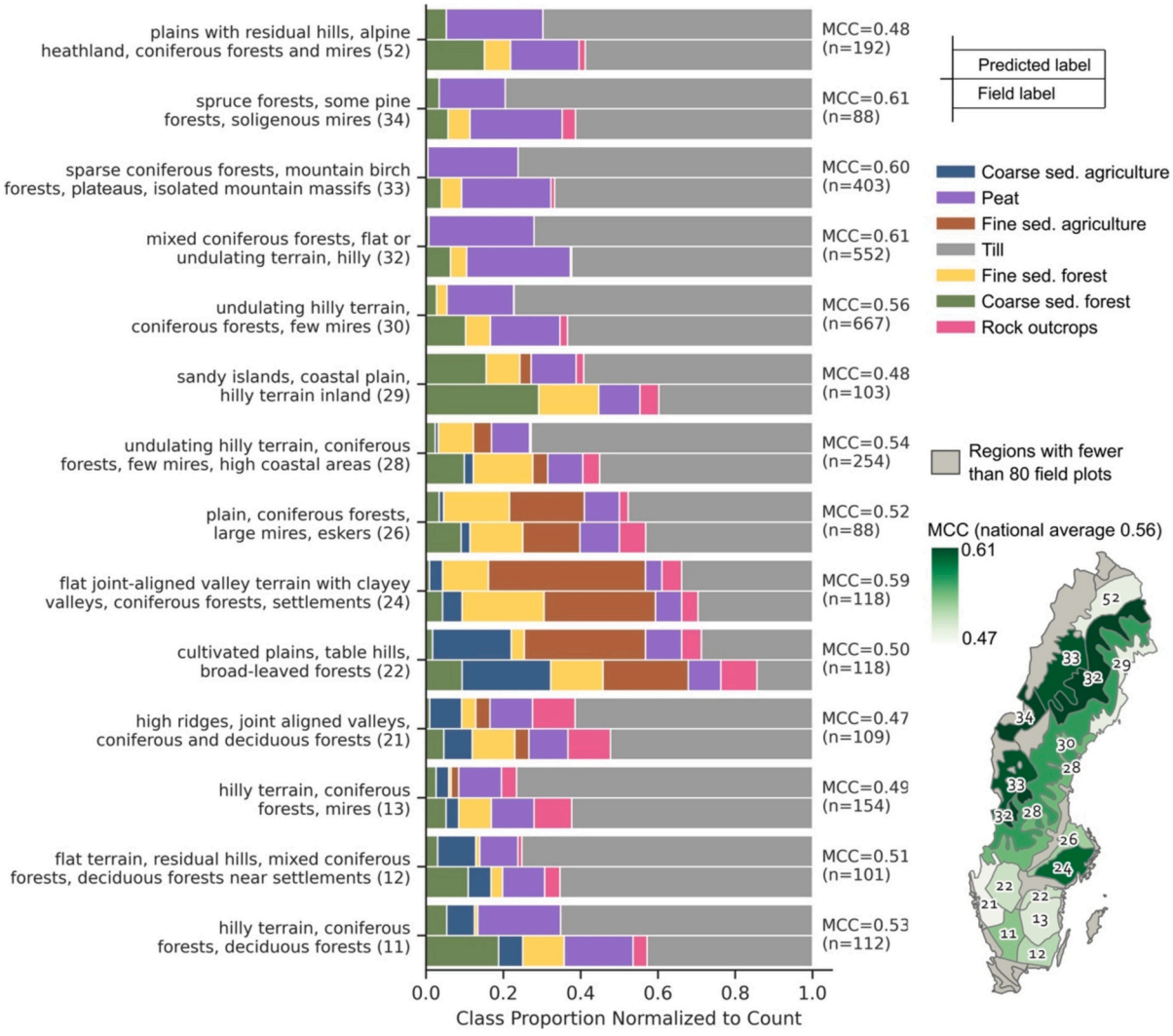

Fig. 5. Spatial variation in model performance across physiographic regions. Only regions with a minimum of 80 field observations were included in the analysis to ensure reliable Matthews Correlation Coefficient (MCC) calculation. The upper bars represent the predicted parent material (PM) class distribution for each region by the XGBoost (all features) model, while the lower bars represent the corresponding distribution of field-observed PM class. The proportion was scaled to sample counts to assist visual comparison.

the XGBoost (all features) model as a complementary tool to accelerate the mapping process in these northern regions.

With the increasing availability of legacy data and open soil databases, future studies are expected to rely more on these resources as a cost-efficient way of soil mapping (Hendriks et al., 2019). However, a key challenge in point-based DSM modeling remains: reconciling the pixel-based nature and the underlying pedogenetic and geomorphic processes of the actual soil landscapes (Rossiter et al., 2022). Although we incorporated features like Distance to the Highest Coastline to indirectly account for the glacial and postglacial processes, a more comprehensive approach may be warranted. Deep learning models, like Unets trained with raster image data may offer a promising avenue by incorporating the contextual information from neighboring cells and extracting multi-scale information automatically (Latifovic et al., 2018; Padarian et al., 2020; Taghizadeh-Mehrjardi et al., 2020), potentially leading to a more physically sound understanding of spatial prediction.

4. Conclusion

This study investigated the potential of Machine Learning (ML) for mapping soil parent materials (PMs) in Sweden, utilizing high-resolution airborne LiDAR data and ancillary maps. Our findings indicated that XGBoost models achieved higher Matthews Correlation Coefficients (MCCs) ranging from 0.45 to 0.56, in contrast to the existing polygon-based Quaternary Deposit (QD) maps, which showed MCCs between 0.18 and 0.36. The high-resolution maps generated by ML approach have the potential to identify previously unmapped smaller PM features. With adequate training data, the XGBoost algorithm successfully extracted valuable insights from the LiDAR data, effectively identifying till and peat. However, its performance decreased for PMs exhibiting high variability in grain size and composition. Regional analyses are crucial for capturing spatial variations in model performance and identifying areas where Digital Soil Mapping (DSM) can complement and enhance conventional mapping methods. Despite these advancements, expertise in soil-landscape relationships remains vital for interpreting model outputs and addressing potential discrepancies with landscape realities.

Funding sources

This work was supported by FORMAS Swedish Research Council for Sustainable Development [grant number 2021–00713, 2021–00115] and Knut and Alice Wallenberg Foundation [grant number 2018.0259 (Future Silviculture)] and partially supported by the Wallenberg AI, Autonomous Systems and Software Program—Humanities and Society (WASP-HS), funded by the Marianne and Marcus Wallenberg Foundation, the Marcus and Amalia Wallenberg Foundation, and Kempestiftelserna.

Declaration of competing interest

The authors declare that they have no known competing financial interests or personal relationships that could have appeared to influence the work reported in this paper.

Acknowledgments

We thank Christofer Engberg Hydén for providing the Swedish Forest Soil Inventory (SFSI) dataset and Johanna Wetterlind for the agricultural soil datasets (SASI).

Appendix A. Supplementary data

Supplementary data to this article can be found online at https://doi.org/10.1016/j.geodrs.2024.e00905.

Data availability

Due to the sensitive nature of the Swedish Forest Soil Inventory plot geocoordinates, the exact data used in this study cannot be publicly shared. The Python codes used to generate the results will be available on GitHub:https://github.com/linyq017/Mapping-Soil-Parent-Materials-in-a-Previously-Glaciated-Landscape

References

Adler, K., Piikki, K., Söderström, M., Eriksson, J., 2022. Digital soil mapping of copper in Sweden: using the prediction and uncertainty as decision support in crop micronutrient management. Geoderma. Reg. 30, e00562. https://doi.org/10.1016/j.geodrs.2022.e00562.

Agrell, H., 1979. The Quaternary of Sweden. Univ. (Sveriges Geologiska Undersökning Serie C, Avhandlingar och uppsatser; 770).

Ågren, A.M., Lin, Y., 2024. A fully automated model for land use classification from historical maps using machine learning. Remote Sens. Appl. Soc. Environ. 36, 101349. https://doi.org/10.1016/j.rsase.2024.101349.

Ågren, A.M., Larson, J., Paul, S.S., Laudon, H., Lidberg, W., 2021. Use of multiple LIDAR-derived digital terrain indices and machine learning for high-resolution national-scale soil moisture mapping of the Swedish forest landscape. Geoderma 404, 115280. https://doi.org/10.1016/j.geoderma.2021.115280.

Ågren, A.M., Hasselquist, E.M., Stendahl, J., Nilsson, M.B., Paul, S.S., 2022. Delineating the distribution of mineral and peat soils at the landscape scale in northern boreal regions. SOIL 8 (2), 733–749. https://doi.org/10.5194/soil-8-733-2022.

Akiba, T., Sano, S., Yanase, T., Ohta, T., Koyama, M., 2019. Optuna: A Next-generation Hyperparameter Optimization Framework. Association for Computing Machinery, New York, NY, USA, pp. 2623–2631. July 25 2019. https://doi.org/10.1145/3292500.3330701.

Anderson, D.W., 1988. The effect of parent material and soil development on nutrient cycling in temperate ecosystems. Biogeochemistry 5 (1), 71–97. https://doi.org/10.1007/BF02180318.

Arrouays, D., Lagacherie, P., Hartemink, A.E., 2017. Digital soil mapping across the globe. Geoderma. Reg. 9, 1–4. https://doi.org/10.1016/j.geodrs.2017.03.002.

Artz, R.R.E., Johnson, S., Bruneau, P., Britton, A.J., Mitchell, R.J., Ross, L., Donaldson-Selby, G., Donnelly, D., Aitkenhead, M.J., Gimona, A., Poggio, L., 2019. The potential for modelling peatland habitat condition in Scotland using long-term MODIS data. Sci. Total Environ. 660, 429–442. https://doi.org/10.1016/j.scitotenv.2018.12.327.

Becher, M., Sohlenius, G., Öhrling, C., 2019. Sur Sulfatjord - Egenskaper Och Utbredning.

Berg, R., 2009. Three-Dimensional Geological Mapping, Workshop Extended Abstracts. https://doi.org/10.13140/RG.2.1.1495.3041.

Bernknopf, R., Brookshire, D., Sollar, D., Mckee, M., Sutter, J., Matti, J., Campbell, R., 1983. Societal Value of Geologic Maps.

Bishop, T.F.A., Horta, A., Karunaratne, S.B., 2015. Validation of digital soil maps at different spatial supports. Geoderma 241–242, 238–249. https://doi.org/10.1016/j.geoderma.2014.11.026.

Blaschke, T., Lang, S., Lorup, E., Strobl, J., Zeil, P., 2000. Object-Oriented Image Processing in an Integrated GIS/Remote Sensing Environment and Perspectives for Environmental Applications.

Blaschke, T., Hay, G.J., Kelly, M., Lang, S., Hofmann, P., Addink, E., Queiroz Feitosa, R., van der Meer, F., van der Werff, H., van Coillie, F., Tiede, D., 2014. Geographic object-based image analysis – towards a new paradigm. ISPRS J. Photogramm. Remote Sens. 87, 180–191. https://doi.org/10.1016/j.isprsjprs.2013.09.014.

Bonfatti, B.R., Demattê, J.A.M., Marques, K.P.P., Poppiel, R.R., Rizzo, R., de Mendes, W. S., Silvero, N.E.Q., Safanelli, J.L., 2020. Digital mapping of soil parent material in a heterogeneous tropical area. Geomorphology 367, 107305. https://doi.org/10.1016/j.geomorph.2020.107305.

Brus, D.J., Kempen, B., Heuvelink, G.B.M., 2011. Sampling for validation of digital soil maps. Eur. J. Soil Sci. 62 (3), 394–407. https://doi.org/10.1111/j.1365-2389.2011.01364.x.

Cavazzi, S., Corstanje, R., Mayr, T., Hannam, J., Fealy, R., 2013. Are fine resolution digital elevation models always the best choice in digital soil mapping? Geoderma 195–196, 111–121. https://doi.org/10.1016/j.geoderma.2012.11.020.

Chen, T., Guestrin, C., 2016. XGBoost: A Scalable Tree Boosting System. In: Proceedings of KDD '16: The 22nd ACM SIGKDD International Conference on Knowledge Discovery and Data Mining, San Francisco California USA, August 13 2016. ACM, pp. 785–794. https://doi.org/10.1145/2939672.2939785.

Chen, S., Arrouays, D., Leatitia Mulder, V., Poggio, L., Minasny, B., Roudier, P., Libohova, Z., Lagacherie, P., Shi, Z., Hannam, J., Meersmans, J., Richer-de-Forges, A. C., Walter, C., 2022. Digital mapping of GlobalSoilMap soil properties at a broad scale: a review. Geoderma 409, 115567. https://doi.org/10.1016/j.geoderma.2021.115567.

Daniels, J., Thunholm, B., 2014. Rikstäckande jorddjupsmodell. (2014:14). https://resource.sgu.se/produkter/sgurapp/s1414-rapport.pdf.

DeLancey, E.R., Kariyeva, J., Bried, J.T., Hird, J.N., 2019. Large-scale probabilistic identification of boreal peatlands using Google Earth Engine, open-access satellite data, and machine learning. PLoS One 14 (6), e0218165. https://doi.org/10.1371/journal.pone.0218165.

Donner, J., Donner, J.J., 2005. The Quaternary History of Scandinavia. Cambridge University Press.

Dowling, T.P.F., Alexanderson, H., Möller, P., 2013. The new high-resolution LiDAR digital height model ('Ny Nationell Höjdmodell') and its application to Swedish quaternary geomorphology. GFF 135 (2), 145–151. https://doi.org/10.1080/11035897.2012.759269.
Ehnvall, B., Ratcliffe, J.L., Bohlin, E., Nilsson, M.B., Öquist, M.G., Sponseller, R.A., Grabs, T., 2023. Landscape constraints on mire lateral expansion. Quat. Sci. Rev. 302, 107961. https://doi.org/10.1016/j.quascirev.2023.107961.
Eilertsen, R.S., Corner, G.D., Hansen, L., 2015. Using LiDAR data to characterize and distinguish among different types of raised terraces in a fjord-valley setting. GFF 137 (4), 353–361. https://doi.org/10.1080/11035897.2015.1111409.
Franzén, L., Lindberg, F., Viklander, V., Walther, A., 2012. The potential peatland extent and carbon sink in Sweden, as related to the Peatland / Ice Age Hypothesis. Mires Peat 10, 1–19.
Ganerød, A.J., Bakkestuen, V., Calovi, M., Fredin, O., Rød, J.K., 2023. Where are the outcrops? Automatic delineation of bedrock from sediments using deep-learning techniques. Appl. Comp. Geosci. 18, 100119. https://doi.org/10.1016/j.acags.2023.100119.
Gillies, S., et al.. Rasterio: Geospatial raster I/O for Python programmers. Mapbox. https://github.com/rasterio/rasterio.
Goodship, A., Alexanderson, H., 2020. Dynamics of a retreating ice sheet: a LiDAR study in Värmland, SW Sweden. GFF 142 (4), 325–345. https://doi.org/10.1080/11035897.2020.1822437.
Gorelick, N., Hancher, M., Dixon, M., Ilyushchenko, S., Thau, D., Moore, R., 2017. Google Earth Engine: Planetary-scale geospatial analysis for everyone. Remote Sensing of Environment 202, 18–27. https://doi.org/10.1016/j.rse.2017.06.031.
Gotway, C.A., Young, L.J., 2002. Combining incompatible spatial data. J. Am. Stat. Assoc. 97 (458), 632–648. https://doi.org/10.1198/016214502760047140.
Gray, J., Murphy, B.W., 1999. Parent Material and Soils: A Guide to the Influence of Parent Material on Soil Distribution in Eastern Australia.
Häggquist, E., Söderholm, P., 2015. The economic value of geological information: synthesis and directions for future research. Res. Policy 43, 91–100. https://doi.org/10.1016/j.resourpol.2014.11.001.
Helmfrid, S., 1996. Geography of Sweden. SNA.
Hendriks, C.M.J., Stoorvogel, J.J., Lutz, F., Claessens, L., 2019. When can legacy soil data be used, and when should new data be collected instead? Geoderma 348, 181–188. https://doi.org/10.1016/j.geoderma.2019.04.026.
Heung, B., Bulmer, C.E., Schmidt, M.G., 2014. Predictive soil parent material mapping at a regional-scale: a random Forest approach. Geoderma 214–215, 141–154. https://doi.org/10.1016/j.geoderma.2013.09.016.
Heung, B., Bulmer, C.E., Schmidt, M.G., Zhang, J., 2022. Provincial-scale digital soil mapping using a random forest approach for British Columbia. Can. J. Soil Sci. 102 (3), 597–620. https://doi.org/10.1139/cjss-2021-0090.
Hudson, B.D., 1992. The soil survey as paradigm-based science. Soil Sci. Soc. Am. J. 56 (3), 836–841. https://doi.org/10.2136/sssaj1992.03615995005600030027x.
Hughes, A.L.C., Gyllencreutz, R., Lohne, Ø.S., Mangerud, J., Svendsen, J.I., 2016. The last Eurasian ice sheets – a chronological database and time-slice reconstruction, DATED-1. Boreas 45 (1), 1–45. https://doi.org/10.1111/bor.12142.
Jenny, H., 1994. Factors of Soil Formation: A System of Quantitative Pedology. Dover.
Johnson, M.D., Fredin, O., Ojala, A.E.K., Peterson, G., 2015. Unraveling Scandinavian geomorphology: the LiDAR revolution. GFF 137 (4), 245–251. https://doi.org/10.1080/11035897.2015.1111410.
Karlson, M., Gålfalk, M., Crill, P., Bousquet, P., Saunois, M., Bastviken, D., 2019. Delineating northern peatlands using Sentinel-1 time series and terrain indices from local and regional digital elevation models. Remote Sens. Environ. 231, 111252. https://doi.org/10.1016/j.rse.2019.111252.
Karlsson, C.S.J., Jamali, I.A., Earon, R., Olofsson, B., Mörtberg, U., 2014. Comparison of methods for predicting regolith thickness in previously glaciated terrain, Stockholm, Sweden. Geoderma 226–227, 116–129. https://doi.org/10.1016/j.geoderma.2014.03.003.
Karlsson, C., Sohlenius, G., Becher, G.P., 2021. Handledning för jordartsgeologiska kartor och databaser över Sverige. (2021:17). The Geological Survey of Sweden.
Knight, J.F., Lunetta, R.S., 2003. An experimental assessment of minimum mapping unit size. IEEE Trans. Geosci. Remote Sens. 41 (9), 2132–2134. https://doi.org/10.1109/TGRS.2003.816587.
Krutskikh, N., 2022. Mapping of the loose sediments of glacial and periglacial formations in areas with boreal vegetation using remote sensing. J. Appl. Remote. Sens. 16, 034528. https://doi.org/10.1117/1.JRS.16.034528].
Larson, J., Lidberg, W., Ågren, A.M., Laudon, H., 2022. Predicting soil moisture conditions across a heterogeneous boreal catchment using terrain indices. Hydrol. Earth Syst. Sci. 26 (19), 4837–4851. https://doi.org/10.5194/hess-26-4837-2022.
Latifovic, R., Pouliot, D., Campbell, J., 2018. Assessment of convolution neural networks for surficial geology mapping in the South Rae geological region, Northwest Territories, Canada. Remote Sens. 10 (2), 307. https://doi.org/10.3390/rs10020307.
Laudon, H., Taberman, I., Ågren, A., Futter, M., Ottosson-Löfvenius, M., Bishop, K., 2013. The Krycklan catchment study—a flagship infrastructure for hydrology, biogeochemistry, and climate research in the boreal landscape. Water Resour. Res. 49 (10), 7154–7158. https://doi.org/10.1002/wrcr.20520.
Laudon, H., Hasselquist, E.M., Peichl, M., Lindgren, K., Sponseller, R., Lidman, F., Kuglerová, L., Hasselquist, N.J., Bishop, K., Nilsson, M.B., Ågren, A.M., 2021. Northern landscapes in transition: evidence, approach and ways forward using the Krycklan catchment study. Hydrol. Process. 35 (4), e14170. https://doi.org/10.1002/hyp.14170.
Lawley, R., Smith, B., 2008. Digital soil mapping at a national scale: A knowledge and GIS based approach to improving parent material and property information. In: Hartemink, A.E., McBratney, A., de Mendonça-Santos, M.L. (Eds.), Digital Soil Mapping with Limited Data. Springer, Netherlands, pp. 173–182. https://doi.org/10.1007/978-1-4020-8592-5_14.
Lemercier, B., Lacoste, M., Loum, M., Walter, C., 2012. Extrapolation at regional scale of local soil knowledge using boosted classification trees: a two-step approach. Geoderma 171–172, 75–84. https://doi.org/10.1016/j.geoderma.2011.03.010.
Lindsay, J., 2024. WhiteboxTools User Manual https://www.whiteboxgeo.com/manual/wbt_book/preface.html?search=2024-07-02.
Liu, X., Zhu, A.-X., Yang, L., Pei, T., Qi, F., Liu, J., Wang, D., Zeng, C., Ma, T., 2022. Influence of legacy soil map accuracy on soil map updating with data mining methods. Geoderma 416, 115802. https://doi.org/10.1016/j.geoderma.2022.115802.
Loiseau, T., Arrouays, D., Richer-de-Forges, A.C., Lagacherie, P., Ducommun, C., Minasny, B., 2021. Density of soil observations in digital soil mapping: a study in the Mayenne region, France. Geoderma Regional 24, e00358. https://doi.org/10.1016/j.geodrs.2021.e00358.
Lundberg, S., Lee, S.-I., 2017. A Unified Approach to Interpreting Model Predictions. arXiv. https://doi.org/10.48550/arXiv.1705.07874.
Matthews, B.W., 1975. Comparison of the predicted and observed secondary structure of T4 phage lysozyme. Biochim. Biophys. Acta (BBA) - Protein Struct. 405 (2), 442–451. https://doi.org/10.1016/0005-2795(75)90109-9.
McBratney, A.B., Mendonça Santos, M.L., Minasny, B., 2003. On digital soil mapping. Geoderma 117 (1), 3–52. https://doi.org/10.1016/S0016-7061(03)00223-4.
McMillan, A.A., 2002. Onshore quaternary geological surveys in the 21st century—a perspective from the British Geological Survey. Quat. Sci. Rev. 21 (8), 889–899. https://doi.org/10.1016/S0277-3791(01)00064-6.
Minarik, R., Hengl, T., Simoes, R., Isik, M.S., Ho, Y.-F., Tian, X., 2024. Soil type (world Reference Base) map of Europe based on ensemble machine learning and multiscale EO data. Res. Square. https://doi.org/10.21203/rs.3.rs-5244083/v1.
Mirzaei, F., Amirian-Chakan, A., Taghizadeh-Mehrjardi, R., Matinfar, H.R., Kerry, R., 2024. Soil textural class modeling using digital soil mapping approaches: effect of resampling strategies on imbalanced dataset predictions. Geoderma. Reg. 38, e00821. https://doi.org/10.1016/j.geodrs.2024.e00821.
Morris, P.J., Swindles, G.T., Valdes, P.J., Ivanovic, R.F., Gregoire, L.J., Smith, M.W., Tarasov, L., Haywood, A.M., Bacon, K.L., 2018. Global peatland initiation driven by regionally asynchronous warming. Proc. Natl. Acad. Sci. 115 (19), 4851–4856. https://doi.org/10.1073/pnas.1717838115.
Mulder, V.L., Lacoste, M., Richer-de-Forges, A.C., Arrouays, D., 2016. GlobalSoilMap France: high-resolution spatial modelling the soils of France up to two meter depth. Sci. Total Environ. 573, 1352–1369. https://doi.org/10.1016/j.scitotenv.2016.07.066.
Nordman, M., Peltola, A., Bilker-Koivula, M., Lahtinen, S., 2020. Past and future Sea level changes and land uplift in the Baltic Sea seen by geodetic observations. In: Freymueller, J.T., Sánchez, L. (Eds.), Beyond 100: The Next Century in Geodesy. Springer International Publishing, pp. 161–167. https://doi.org/10.1007/1345_2020_124.
O'Leary, D., Brown, C., Daly, E., 2022. Digital soil mapping of peatland using airborne radiometric data and supervised machine learning – implication for the assessment of carbon stock. Geoderma 428, 116086. https://doi.org/10.1016/j.geoderma.2022.116086.
Padarian, J., Minasny, B., McBratney, A.B., 2020. Machine learning and soil sciences: a review aided by machine learning tools. SOIL 6 (1), 35–52. https://doi.org/10.5194/soil-6-35-2020.
Pedregosa, F., Varoquaux, G., Gramfort, A., Michel, V., Thirion, B., Grisel, O., Blondel, M., Prettenhofer, P., Weiss, R., Dubourg, V., Vanderplas, J., Passos, A., Cournapeau, D., Brucher, M., Perrot, M., Duchesnay, É., 2011. Scikit-learn: Machine Learning in Python. J. Machine Learning Res. 12 (85), 2825–2830 [2024-08-15]. http://jmlr.org/papers/v12/pedregosa11a.html.
Peterson, G., Johnson, M.D., Smith, C.A., 2017. Glacial geomorphology of the south Swedish uplands – focus on the spatial distribution of hummock tracts. J. Maps 13 (2), 534–544. https://doi.org/10.1080/17445647.2017.1336121.
Piedallu, C., Pedersoli, E., Chaste, E., Morneau, F., Seynave, I., Gégout, J.-C., 2022. Optimal resolution of soil properties maps varies according to their geographical extent and location. Geoderma 412, 115723. https://doi.org/10.1016/j.geoderma.2022.115723.
Piikki, K., Söderström, M., 2019. Digital soil mapping of arable land in Sweden – validation of performance at multiple scales. Geoderma 352, 342–350. https://doi.org/10.1016/j.geoderma.2017.10.049.
Piilo, S.R., Korhola, A., Heiskanen, L., Tuovinen, J.-P., Aurela, M., Juutinen, S., Marttila, H., Saari, M., Tuittila, E.-S., Turunen, J., Väliranta, M.M., 2020. Spatially varying peatland initiation, Holocene development, carbon accumulation patterns and radiative forcing within a subarctic fen. Quat. Sci. Rev. 248, 106596. https://doi.org/10.1016/j.quascirev.2020.106596.
Prince, A., Franssen, J., Lapierre, J.-F., Maranger, R., 2020. High-resolution broad-scale mapping of soil parent material using object-based image analysis (OBIA) of LiDAR elevation data. CATENA 188, 104422. https://doi.org/10.1016/j.catena.2019.104422.
Ramcharan, A., Hengl, T., Nauman, T., Brungard, C., Waltman, S., Wills, S., Thompson, J., 2018. Soil property and class maps of the conterminous United States at 100-meter spatial resolution. Soil Sci. Soc. Am. J. 82 (1), 186–201. https://doi.org/10.2136/sssaj2017.04.0122.
Richer-de-forges, A.C., Arrouays, D., Poggio, L., Chen, S., Lacoste, M., Minasny, B., Libohova, Z., Roudier, P., Mulder, V.L., Nédélec, H., Martelet, G., Lemercier, B., Lagacherie, P., Bourennane, H., 2022. Hand-feel soil texture observations to evaluate the accuracy of digital soil maps for local prediction of particle size distribution. A case study in Central France. Pedosphere. https://doi.org/10.1016/j.pedsph.2022.07.009.

Richter, J., Owens, P., Libohova, Z., Adhikari, K., Fuentes, B., 2019. Mapping parent material as part of a nested approach to soil mapping in the Arkansas River Valley. Catena 178, 100–108. https://doi.org/10.1016/j.catena.2019.02.031.

Rimondini, L., Gumbricht, T., Ahlström, A., Hugelius, G., 2023. Mapping of peatlands in the forested landscape of Sweden using LiDAR-based terrain indices. ESSD – Land/Pedol. https://doi.org/10.5194/essd-2023-77.

Roering, J.J., Mackey, B.H., Marshall, J.A., Sweeney, K.E., Deligne, N.I., Booth, A.M., Handwerger, A.L., Cerovski-Darriau, C., 2013. 'You are HERE': connecting the dots with airborne lidar for geomorphic fieldwork. Geomorphology 200, 172–183. https://doi.org/10.1016/j.geomorph.2013.04.009.

Rossiter, D.G., Poggio, L., Beaudette, D., Libohova, Z., 2022. How well does digital soil mapping represent soil geography? An investigation from the USA. Soil 8 (2), 559–586. https://doi.org/10.5194/soil-8-559-2022.

Salazar Rincón, Á.E., Rodríguez García, J.A., Cañas, V., Sevillano Matilla, A., Galindo Jiménez, I., Sánchez Jiménez, N., 2019. Quaternary geological mapping in Spain and contribution to the update of the International Quaternary Map of Europe https://digital.csic.es/handle/10261/2738132024-08-30.

Sayidov, A., Aliakbarian, M., Weibel, R., 2020. Geological map generalization driven by size constraints. ISPRS Int. J. Geo Inf. 9 (4), 284. https://doi.org/10.3390/ijgi9040284.

Sharififar, A., Sarmadian, F., Malone, B.P., Minasny, B., 2019. Addressing the issue of digital mapping of soil classes with imbalanced class observations. Geoderma 350, 84–92. https://doi.org/10.1016/j.geoderma.2019.05.016.

Smirnoff, A., Huot-Vézina, G., Paradis, S.J., Boivin, R., 2012. Generalizing geological maps with the GeoScaler software: the case study approach. Comput. Geosci. 40, 66–86. https://doi.org/10.1016/j.cageo.2011.07.013.

Söderström, M., Sohlenius, G., Rodhe, L., Piikki, K., 2016. Adaptation of regional digital soil mapping for precision agriculture. Precis. Agric. 17 (5), 588–607. https://doi.org/10.1007/s11119-016-9439-8.

Sorenson, P.T., Kiss, J., Bedard-Haughn, A.K., 2023. Improved parent material map disaggregation methods in the Saskatchewan prairies using historical bare soil composite imagery. Can. J. Soil Sci. 103 (1), 47–63. https://doi.org/10.1139/cjss-2021-0154.

Statistics Sweden, R. aand E.D, 2019. Markanvändningen i Sverige.

Stroeven, A.P., Hättestrand, C., Kleman, J., Heyman, J., Fabel, D., Fredin, O., Goodfellow, B.W., Harbor, J.M., Jansen, J.D., Olsen, L., Caffee, M.W., Fink, D., Lundqvist, J., Rosqvist, G.C., Strömberg, B., Jansson, K.N., 2016. Deglaciation of Fennoscandia. Quat. Sci. Rev. 147, 91–121. https://doi.org/10.1016/j.quascirev.2015.09.016.

Taghizadeh-Mehrjardi, R., Mahdianpari, M., Mohammadimanesh, F., Behrens, T., Toomanian, N., Scholten, T., Schmidt, K., 2020. Multi-task convolutional neural networks outperformed random forest for mapping soil particle size fractions in Central Iran. Geoderma 376, 114552. https://doi.org/10.1016/j.geoderma.2020.114552.

Teng, H., Viscarra Rossel, R.A., Shi, Z., Behrens, T., 2018. Updating a national soil classification with spectroscopic predictions and digital soil mapping. CATENA 164, 125–134. https://doi.org/10.1016/j.catena.2018.01.015.

The Geological Survey of Sweden, 2015. hogsta-kustlinjen-beskrivning.pdf. https://resource.sgu.se/dokument/produkter/hogsta-kustlinjen-beskrivning.pdf.

The Geological Survey of Sweden, 2018. jordarter-750000-mittnorden-beskrivning. https://resource.sgu.se/dokument/produkter/jordarter-750000-mittnorden-wms-beskrivning.pdf.

The Geological Survey of Sweden, 2023. jorddjupsmodell-beskrivning.pdf. https://resource.sgu.se/dokument/produkter/jorddjupsmodell-beskrivning.pdf [2023-11-30].

The Geological Survey of Sweden (2024a). jordarter-25-100000-beskrivning. https://resource.sgu.se/dokument/produkter/jordarter-25-100000-beskrivning.pdf.

The Geological Survey of Sweden (2024b). jordarter-1miljon-beskrivning. https://resource.sgu.se/dokument/produkter/jordarter-1miljon-beskrivning.pdf.

The Geological Survey of Sweden (2024c). jordarter-200000-vasternorrland-beskrivning. https://resource.sgu.se/dokument/produkter/jordarter-200000-vasternorrland-beskrivning.pdf.

The Geological Survey of Sweden (2024d). jordarter-250000-nordligaste-sverige-beskrivning. https://resource.sgu.se/dokument/produkter/jordarter-250000-nordligaste-sverige-beskrivning.pdf.

The Swedish Environmental Protection Agency, 2020. National Land Cover Database (NMD) - Product Description.

The Swedish Land Survey, 2022. Quality Description Laser Data.

The Swedish National Forest Inventory, 2021. Fieldwork Instructions. Riksinventeringen av skog. https://www.slu.se/globalassets/ew/org/centrb/rt/dokument/faltinst/nfi_fieldwork_instructions_eng.pdf.

Wadoux, A.M.J.-C., Minasny, B., McBratney, A.B., 2020. Machine learning for digital soil mapping: applications, challenges and suggested solutions. Earth Sci. Rev. 210, 103359. https://doi.org/10.1016/j.earscirev.2020.103359.

Watanabe, S., 2023. Tree-Structured Parzen Estimator: Understanding its Algorithm Components and Their Roles for Better Empirical Performance. arXiv. https://doi.org/10.48550/arXiv.2304.11127.

Webster, T.L., Murphy, J.B., Gosse, J.C., Spooner, I., 2006. The application of lidar-derived digital elevation model analysis to geological mapping: an example from the Fundy Basin, Nova Scotia, Canada. Can. J. Remote. Sens. 32 (2), 173–193. https://doi.org/10.5589/m06-017.

Weerts, H.J.T., Westerhoff, W.E., Cleveringa, P., Bierkens, M.F.P., Veldkamp, J.G., Rijsdijk, K.F., 2005. Quaternary geological mapping of the lowlands of the Netherlands, a 21st century perspective. Quat. Int. 133–134, 159–178. https://doi.org/10.1016/j.quaint.2004.10.011.

Whiteside, T.G., Boggs, G.S., Maier, S.W., 2011. Comparing object-based and pixel-based classifications for mapping savannas. Int. J. Appl. Earth Obs. Geoinf. 13 (6), 884–893. https://doi.org/10.1016/j.jag.2011.06.008.

Wu, Q., 2020. geemap: A Python package for interactive mapping with Google Earth Engine. J. Open Source Software 5 (51), 2305. https://doi.org/10.21105/joss.02305.

Wulder, M.A., White, J.C., Luther, J.E., Strickland, G., Remmel, T.K., Mitchell, S.W., 2006. Use of vector polygons for the accuracy assessment of pixel-based land cover maps. Can. J. Remote. Sens. 32 (3), 268–279. https://doi.org/10.5589/m06-023.

Zhang, G., Liu, F., Song, X., 2017. Recent progress and future prospect of digital soil mapping: a review. J. Integr. Agric. 16 (12), 2871–2885. https://doi.org/10.1016/S2095-3119(17)61762-3.